

Enhancing accuracy of uncertainty estimation in appearance-based gaze tracking with probabilistic evaluation and calibration

Qiaojie Zheng
Colorado School of Mines
1500 Illinois St. Golden CO, USA
zheng@mines.edu

Jiucui Zhang
Colorado School of Mines
1500 Illinois St. Golden CO, USA
zhangjiucui@gmail.com

Xiaoli Zhang
Colorado School of Mines
1500 Illinois St. Golden CO, USA
xlzhang@mines.edu

Abstract

Accurately knowing uncertainties in appearance-based gaze tracking is critical for ensuring reliable downstream applications. Due to the lack of individual uncertainty labels, current uncertainty-aware approaches adopt probabilistic models to acquire uncertainties by following distributions in the training dataset. Without regulations, this approach lets the uncertainty model build biases and overfits the training data, leading to poor performance when deployed. We first presented a strict proper evaluation metric from the probabilistic perspective based on comparing the coverage probability between prediction and observation to provide quantitative evaluation for better assessment on the inferred uncertainties. We then proposed a correction strategy based on probability calibration to mitigate biases in the estimated uncertainties of the trained models. Finally, we demonstrated the effectiveness of the correction strategy with experiments performed on two popular gaze estimation datasets with distinctive image characteristics caused by data collection settings.

1. Introduction

Appearance-based gaze tracking is a task full of uncertainties[21]. Factors such as appearance of subjects, lighting conditions, and camera parameters can greatly affect the model's performance[19]. For reliable downstream mission-critical decision-making applications, such as driver monitoring systems, only knowing point estimations of gaze angles are insufficient, the accompanied inference uncertainties must also be provided to assess the trustworthiness/confidence of the gaze tracking result.

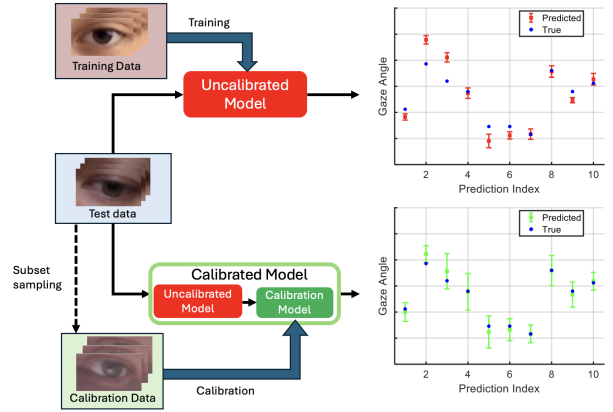


Figure 1. Inaccuracies of existing uncertainty-aware gaze tracking model and the proposed remedy plan. Uncertainty estimations from existing models provide inaccurate prediction ranges and often cannot capture the ground truth gaze angle values (black dot) because of strong biases towards the training data from the uncertainty model. We proposed to introduce a calibration model to compensate for the bias behavior to generate accurate uncertainty estimates such that majority of the ground truth value of gaze angles can be captured for better downstream decision making.

Equipping models with uncertainty awareness is a challenging task since the ground truth values of uncertainties are not available for each individual training sample. To circumvent this challenge, current methods typically employ a probabilistic approach such that the trained model outputs a probabilistic description of gaze angles that resembles the overall probabilistic distribution of the training dataset[12, 13]. Variances, or prediction ranges, from the probabilistic prediction represents the uncertainty level

– higher variances signal higher uncertainties[10].

Despite allowing the model to acquire uncertainty inference capabilities, this training approach faces significant limitations. By letting the model adhere to the probability distribution from training data, the current training approach essentially treated the training data distribution as the uncertainty ground truth, allowing strong biases toward the training data [12]. Since distribution from the testing data rarely follows that of the training data, such bias leads to inaccuracies in uncertainty estimation results, hindering broader applications of current uncertainty-aware models.

Even more critically, existing metric and assessment approach for the inferred uncertainties failed to reveal the bias issue because they rely on an improper scoring rule developed from a spurious correlation between the gaze angle inference error and the estimated uncertainties (error-uncertainty correlation in short). By relying on the error-uncertainty correlation, existing studies essentially assume that errors in gaze angle have a strict positive correlation with uncertainties. Such a strict correlation is unlikely because uncertainties are not caused by prediction errors in gaze angles. Uncertainties only originate from two sources – aleatoric (data-related) and epistemic (model-related) ones, but no error-related ones[11]. Therefore, the error-uncertainty correlation is an improper scoring metric and cannot effectively and quantitatively reflect inaccuracies in uncertainty estimation.

To comprehensively evaluate the inferred uncertainty and fix the bias problem, in this work, we first proposed a strictly proper scoring metric, inspired by Brier score[2], for assessing the inferred uncertainty based on the idea of coverage probability. This score provides the differences between the coverage probabilities calculated from the predicted probabilistic distribution and that from the empirical observation of the testing data. Next, we proposed a workflow based on probabilistic calibration to compensate for inaccuracy of uncertainty estimations from the original model (referred to as the uncalibrated model). The probabilistic calibration process enforces a match between predicted and observed probability distributions. After that, we conducted uncertainty calibration experiments with two datasets collected under distinctive collection settings to demonstrate the effectiveness of our calibration process. Experiment results also revealed that the uncertainty calibration process also introduces side benefits in slightly increase gaze angle prediction accuracies. Finally, we showed a case study that demonstrated the limitations of existing uncertainty-aware models and the practical application of the calibration process.

The concept of the calibration process is illustrated in Figure 1. Specifically, we introduced a relatively independent calibration model attached to the existing uncertainty-aware models. With a few post-hoc calibration samples,

collected from the testing domain, the calibration model learns the bias behavior in uncalibrated uncertainty models and applies corrections accordingly. In short, we summarize out contributions as follows:

1. Introduced a strictly proper evaluation metric for thorough assessment of the inferred uncertainties in appearance-based gaze tracking, revealing the bias problem of the current uncertainty-aware model.
2. Introduced a correctional model to fix the bias issue in uncertainty estimation in current appearance-based gaze tracking models.
3. Demonstrated the effectiveness of correction with two deep learning backbone structures and two datasets. Showcased the practical application of the calibration with case study.

2. Related Work

2.1. Appearance-Based Gaze Tracking

Appearance-based gaze tracking is a computer vision technique that predicts a person’s gaze angle directly from images of their eyes or faces with deep learning models, without requiring explicit feature extractions like pupil or corneal reflections [18]. With the advancement of large gaze-tracking dataset, such as Columbia Gaze[17], MPII[19, 20], and RTGene[5], and the introduction of powerful models[3, 15, 20], estimating appearance-based gaze tracking can achieve angular accuracies in the range of 4-6 degrees for high image quality datasets and around 7-10 degrees for low image quality datasets.

Differences in training and testing data naturally pose challenges in achieving accurate gaze tracking results. Under some circumstances, such as collection environment changes across different datasets, the tracking accuracy can witness significant drop. To solve this issue, existing approaches[15] implemented meta learning to adapt gaze tracking models to better fit the testing data and achieved the state-of-the-art angular accuracies of 3.14 degrees in MPII gaze dataset.

2.2. Uncertainty-Aware Appearance-Based Gaze Tracking

More recent studies have started to focus on estimating uncertainties aiming to provide more informative gaze tracking results for downstream applications. With appropriate uncertainty estimations, the inappropriate inferences results may be discarded to prevent bad decisions. Several approaches have been proposed, such as quantile regression[10], Confidence Gated Units[9], have been proposed to obtain uncertainty estimations. Further applications, such as outlier detection[4], trust score assignment[9] have been made possible by the introduction of uncertainty awareness.

Similar to the gaze angle estimation problem in Section 2.1, performances of uncertainty estimation are also affected by the differences in training and testing data, except this problem is more severe in uncertainty case due to the lack of regulation during training. As mentioned in Section 1, relying on probability distribution for uncertainty learning leads to strong bias toward the training data, resulting in poor performance during testing. Due to the lack of ground truth for uncertainty values, the typical meta learning approach is not suitable. Moreover, the bias problem in uncertainty estimation was unnoticed due to the lack of proper quantitative evaluation approach. Existing error-uncertainty correlation described in Section 1 can only provide qualitative assessment without conclusive evaluations. Although most existing works[9, 10] reported the nonlinear correlations between inferred uncertainties and angular prediction to be in the range of 0.4 to 0.6, no conclusion can be made solely based on this value. Numerical differences cannot demonstrate the superiority of one model over the other, as angular prediction errors does not cause uncertainties directly. As a result, domain adaptations for the uncertainty-aware model have not been developed, limiting the development of more reliable uncertainty-aware models for broader application.

3. Method and Metric

3.1. Strictly Proper Scoring Metric for Evaluating Uncertainty

A proper scoring metric is necessary to quantitatively evaluate the accuracy of the inferred uncertainty from models. A strictly proper metric only assigns the best score to the only optimal model[7]. For evaluating the predicted uncertainties, the proper scoring rule will reach the optimum when the predicted probability distributions match those from empirical observations. Comparing the cumulative distribution functions (CDF) provides a full distribution for thorough comparison, and it is also easy to develop a proper metric with[16]. We begin the metric development by evaluating pointwise discrepancy (error) between the two CDFs at a single probability value. This discrepancy is described by Equation 1. In this equation θ_t denotes the ground truth gaze angle value for the t^{th} input sample (we denote it as x_t for the rest of the paper), p is a specified probability value in the range of $[0, 1]$, T is the total number of samples involved, F_t denotes the predicted CDF corresponding to input sample x_t , F_t^{-1} is therefore the quantile function (inverse CDF) that calculated the quantile value based on input probability, I here denotes indicator function that equals to 1 when the condition is satisfied and 0 otherwise. $\sum_{t=1}^T \frac{I\{\theta_t \leq F_t^{-1}(p)\}}{T}$ represents the probability that the ground truth angle values fall within the prediction boundary, calculated with the quantile function on specified

probability p , we describes this term as empirical probability from observation in short. For simplicity, we will denote this term as $\hat{P}(p)$

Small error means that the predicted CDF is close to the true data distribution. Because gaze angles contain two angular components, pitch and yaw, the term inside of indicator function $\theta_t \leq F_t^{-1}(p)$ needs to be satisfied for both components for the condition to be considered as satisfied.

$$p_{err}(p) = \left| p - \sum_{t=1}^T \frac{I\{\theta_t \leq F_t^{-1}(p)\}}{T} \right| \quad (1)$$

For evaluation of the overall distribution discrepancy, this difference needs to be evaluated over the entire probability range of $[0, 1]$. To simplify the calculation, inspired by Brier score, here, we will use discrepancies evaluated at 11 probability points ranging from 0 to 1 with an increment of 0.1 to approximate the evaluation. The root mean squared differences of these 11 points (we refer to this value as Coverage Probability Error, CPE in short) are used to represent the overall uncertainty accuracy, higher values correspond to lower uncertainty accuracy, as shown in Equation 2. The perfect uncertainty model, i.e., predicted CDF matches observed exactly, will reach a minimum CPE value of 0, following the definition of strict proper scoring rule.

$$CPE = \sqrt{\frac{1}{10} \sum_{i=0}^{10} p_{err}(0.1i)^2} \quad (2)$$

3.2. Uncertainty Model Calibration

Uncertainty models with high CPE values are inaccurate and are formally referred to miscalibrated models. Miscalibration can lead to issues of misplaced confidence, such as the overconfident example demonstrated in Figure 2. In this example, we would expect that the prediction region would provide a cumulative probability of 90%, but in reality, we can only observe a probability of 80%. This error leads to overconfident estimations, which produces underestimated uncertainties.

To correct the miscalibration issue, one approach is to offset errors before inferencing. For example, if we aim to determine the quantile value corresponding to a probability of 0.9, but our model is miscalibrated and must predict at a probability of 0.95 to match the real-world quantile for 0.9, we can leverage this insight by instructing the model to predict at 0.95 whenever our true target is the 0.9 quantile. In the probability calibration case, we would introduce a secondary regressor model R to incorporate the desired mapping described in the example above. Formally, this regressor creates a mapping $R : [0, 1] \rightarrow [0 : 1]$, that maps probability in the miscalibrated and biased domain into a calibrated and proper domain, such that it allows the corrected CDF, $R \circ F$, to accurately reflect the true data dis-

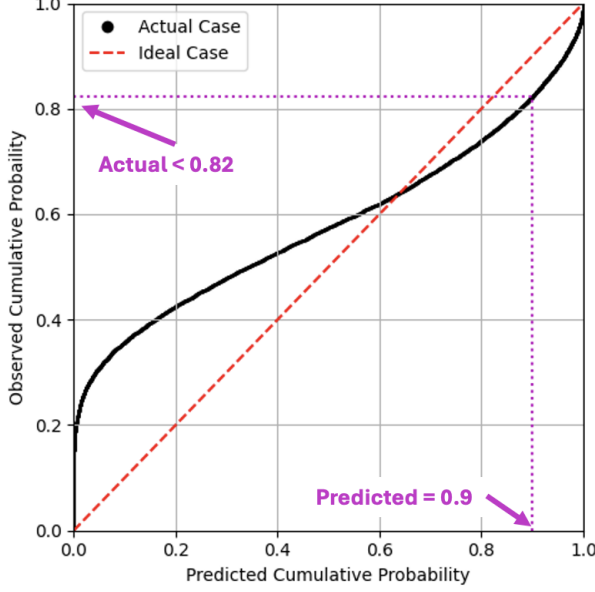


Figure 2. Demonstration of uncertainty inaccuracy causes. The predicted cumulative probability distribution is different from the actual cumulative probability distribution from observation, deviating from the idea case (red dashed line). When model predicted cumulative probability distribution to be 0.9 the real probability is less than 0.82, leading to overconfident estimation or underestimation of uncertainties.

tribution. The objective to train such correctional regressor is described by Equation 3 where p_i is the uncalibrated predicted probability for the i^{th} sample from an ordered group such that $p_i \leq p_{i+1}$. Such ordering is necessary to express the monotonic increasing nature of any CDF, even if uncalibrated. The correction model R needs to satisfy this requirement such that $R(p_i) \leq R(p_{i+1})$ for any realistic corrections.

$$\min \sum_{i=1}^T \left\| \hat{P}(p_i) - R(p_i) \right\|, \quad (3)$$

s. t. : $R(p_i) \leq R(p_{i+1}) \forall p_i \leq p_{i+1}$

During application, the threshold is determined based on the error-adjusted probability $R^{-1}(p)$, instead directly on the original p value. This ensures that predictions aligns more closely with true values, as described in equation 4. Therefore, the calibrated ones are described as $\hat{P}(R^{-1}(p))$.

$$\sum_{t=1}^T \frac{I \{ \theta_t \leq F_t^{-1}(R^{-1}(p)) \}}{T} \rightarrow p \quad (4)$$

To train such calibration regressor model R , we need a dataset $D = \left\{ (p_i, \hat{P}(p_i)) \right\}$, $i = 1..n$, that will ideally

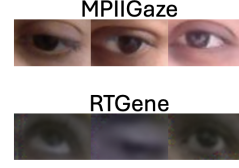


Figure 3. Visualization of MPIIGaze and RTGene dataset samples. Samples in RTGene is much noisier than the MPIIGaze image. Difference in the two dataset provides sharp probability distribution to test the effectiveness of calibration.

capture all error behaviors of the uncalibrated CDF over the entire range of $[0, 1]$ for p . However, this is challenging because we cannot directly sample based on p values; instead, we can only sample the input x . In this study, we performed a random sampling from the testing dataset to form a subset for obtaining the calibration model. By forming the subset, we assume that the subset captures the overall probability distribution in the data.

After acquiring the training data, we will build the calibration model R with an isotonic regression approach to comply with the monotonic nature of CDF. The isotonic regression will return a simple, non-parametric calibration model R that barely adds additional computational overhead to existing deep learning models. Additionally, the non-parametric nature also free the uncalibrated CDF from the constraint from distribution assumption from the main uncertainty-aware model and take any other forms that better match the true data distribution. Median values are used to represent the point estimation for gaze angles rather than the mean valued used for describing the normal distribution. To cope with the two-component nature of the gaze vector, the calibration process was performed individually to each of the component.

For the uncertainty-aware gaze tracking specifically, the calibration process is performed independently and individually to the pitch and yaw components.

4. Experiments

4.1. Experiment Dataset

MPIIGaze[19] and RTGene[5] gaze dataset are the two datasets used in this study, they differ significantly in data collection methods and quality. The significant differences let these two datasets to have distinctive data distribution, allowing a thorough evaluation of the model calibration process. Images from the MPIIGaze and RTGene are provided in Figure 3. for quality visualization.

MPIIGaze consists of 213,695 images from 15 participants, captured under common laptop-use conditions with camera-subject distances around 0.5m. This collection condition yields most of the images to contain clear eye fea-

tures.

In contrast, images from the RTGene dataset are much noisier and contain blurred eye features due to greater camera-subject distances ranging from 0.5 to 2.9m. Additionally, a generative adversarial network (GAN) inpainting process to remove the data collection glasses. As a result, the RTGene data set contains images with much higher noise levels with less clear eye features. These sharp differences in data characteristics make probability distributions from these two datasets significantly different, providing environment for thorough evaluation for the effectiveness of calibration process.

4.2. Uncertainty-Aware Deep Learning Gaze Tracking Structure

The uncertainty-aware gaze estimation used in this study is a heteroskedastic regression model that provides a probabilistic description of the gaze angle[14]. This regression model assumes that gaze angles follow Gaussian distributions and outputs mean and variance estimations to describe the distribution. Specifically, the training process helps to construct a forecaster H and takes in inputs x_t , composed of left eye patch, right eye patch, and head angle readings and output two Gaussian distribution, described by means value $H_{\theta,yaw}(x_t)$, $H_{\theta,pitch}(x_t)$ and variance values $H_{\sigma,yaw}^2(x_t)$, $H_{\sigma,pitch}^2(x_t)$ respectively, as illustrated in Figure 4. For simplicity, we referred to the estimated mean gaze values as $\hat{\theta}_t$ and the variances as $\hat{\sigma}_t^2$, the estimated mean and variance each contains two values for pitch and yaw component respectively. The true values for gaze angles are denoted as θ_t . We implemented two variations of the network with different backbone structure – Resnet 18 and Resnet 50 to provide thorough evaluations.

The loss function employed is a negative log-likelihood (NLL) function (Equation 5) described by a heteroskedastic Gaussian distribution with mean and variances. l_n is the prediction error on the mean value. For training stability, we used L1 loss (Equation 6) to measure the prediction error. The NLL loss function allows training without variance labels by assuming the output follows a normal distribution. While the true values and their distribution may deviate from a strict normal distribution, assuming simple parametric forms facilitates the quick calculation of probability functions. This approach helps avoid the significant computational cost of implementing Monte Carlo dropout[6] or complexity of implement a Bayesian neural networks [1, 8]for uncertainty approximation.

$$NLL_t = \frac{1}{2} \ln(\hat{\sigma}_t^2) + \frac{l_{n,t}}{2\hat{\sigma}_t^2} \quad (5)$$

$$l_{n,t} = \begin{cases} 0.5(\hat{\theta}_t - \theta_t)^2, & \text{for } |\hat{\theta}_t - \theta_t| < 1 \\ |\hat{\theta}_t - \theta_t| - 0.5, & \text{otherwise} \end{cases} \quad (6)$$

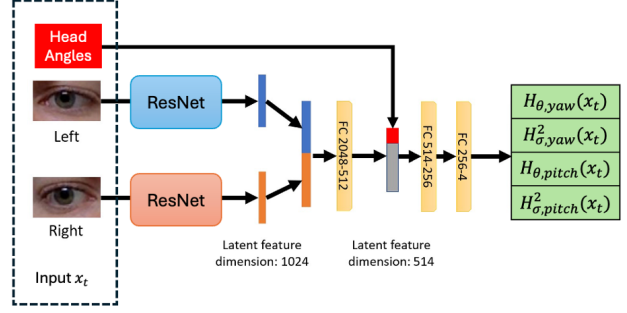


Figure 4. The uncertainty-aware appearance-based gaze estimation structure used in the experiments. The model takes inputs of left and right eye patches together with head angles to output two normal distributions to describe the gaze angle estimates. Mean values are angular estimates, and variances represent uncertainty.

Table 1. Evaluation Configurations

Dataset	Validation Folds	CNN backbone
MPIIGaze RTGene	3	Resnet 18/Resnet 50

4.3. Evaluation Cases

We evaluate the effectiveness of the calibration approach under both within-dataset and cross-dataset testing cases. These two testing cases allow the evaluation method and calibration model to experience different levels of probability distribution change, allowing for thorough assessment. Training, validation, calibration and testing data all originate from the same dataset in the within-dataset case. In cross-dataset case, origins of the training and validation differs from that of the calibration and testing data. The calibration data is composed of 100 images randomly selected from the testing data group and were not involved in the final testing. For each testing cases with each backbone models, a 3-fold cross validation evaluation approach was performed. In total, 12 evaluations, listed in Table 1, were performed with different combinations of subjects, datasets, and models. The average value and span of the CPE were used to evaluate the uncertainty estimation performance. Angular errors were also reported to study the effects of calibration on angular prediction accuracy.

4.4. Case Study

The testing cases provide individual evaluations on the accuracies of angular accuracies and inference accuracies, but it may be difficult to see the practical benefits of the calibration process. Here we further included a case showcase the potential of accurately acquiring the appropriate confidence intervals with the calibrated model.

The most common application of case study is the use

of confidence intervals. 95% confidence interval is one of the most commonly used intervals for high-accuracy uncertainty-related applications. For a symmetric confidence interval, the lower and upper bound for the 95% confidence interval were selected to be 2.5% and 97.5%. For a well-calibrated and reliable model, we expect the predicted quantile limits from the uncertainty-aware model to capture 95% of all labeled gaze angle values. Mathematically, this expectation can be expressed as equation 7, which is two-sided modification from equation 3. In this equation, p_l and p_u represent the lower and upper bound corresponds to the desired confidence interval p_{CI} . In this case study, $p_u = 0.975$, $p_l = 0.025$, and $p_{CI} = 0.95$.

$$\sum_{t=1}^T \frac{I \{F_t^{-1}(p_l) \leq \theta_t \leq F_t^{-1}(p_u)\}}{T} \rightarrow p_{CI} \quad (7)$$

For thorough comparison, we include the uncalibrated heteroskedastic regression model and quantile regression (trained with pinball loss) as baseline for performance comparison. It should be noted that quantile regression only provides limited number of quantile points estimates rather than a complete distribution, thus, it is not suitable for calibration process described in Section 3.2. The case study will showcase the accuracy of the uncertainty models in acquiring a 95% confidence interval under the setting of within-dataset testing for both the MPIIGaze and RTGene dataset. It should be noted that while it is possible to configure the quantile regression to output predictions at the 11 quantile points as needed by the proposed CPE evaluation metric, we found out that such configuration will easily let the quantile regression model lose accuracy. Therefore, the quantile regression model is only involved in the case study to output two values.

Prediction ranges magnitudes corresponds to the 95% confidence interval are also reported in the case study. This value will also provide additional insights in judging the uncertainty-awareness qualitatively. Larger prediction ranges generally corresponds to higher levels of uncertainties.

5. Results

5.1. Coverage Probability Error and Angular Error

Angular errors, average CPE and correlations scores across the 3-fold validation is summarized in Table 2. Both angular error and CPE witnessed decrease with the calibration process. It should be noted that the error-uncertainty correlation only went through negligible change from the correction in inferences in angular value. These changes were not significant to show through the rounded numbers reported in the table, and thus, they reported once. Additionally, we can no longer conclude the uncertainty with a

single parameter over the entire probability range due to the non-parametric correction regressor R . Prior to the calibration, the uncertainty values can be described by a single value, which is the variance related to the CDF F . After the calibration, the “variance” is no longer constant across different regions over the probability range. Additionally, any scaling applied by the correction regressor R will be uniform across all samples in the dataset for a specific p value, and hence, correlation will not change.

When comparing CPE improvement, the cross-dataset experiments generally showed greater gains than the within-dataset case due to the stark differences in probability distributions between the two datasets, which stem from variations in data collection setups. It is interesting to note that the within-dataset test performed on RTGene data saw the smallest improvement. This means that the uncalibrated data is approximately accurate to begin with. This behavior may be attributed to the universal high noise and GAN artifacts exist in all data samples that the probability distribution across different subjects is similar. The uncertainty-aware models were able to accurately capture these features and output accurate uncertainty estimations. On the contrary, models trained on MPII experienced greater improvement from the calibration step. We think that the sharp image quality and clear eye features caused distinctive probability distributions between training and testing data. Overfitting and bias towards to training data caused poor uncertainty model performance to begin with.

Comparing the error-uncertainty correlation to uncalibrated CPEs, we can see that the evaluation results are roughly rank appropriate in the within-dataset (top 4) testing case: models with high error-uncertainty correlation tend to have lower CPE values. However, when larger differences are introduced into the test case, as in the cross-dataset testing (bottom 4 rows), the rank appropriateness no longer holds true.

To help understand the correction mechanism, we created plot showing the probability distribution comparison between the prediction and observation. This figure showed on of the three fold testings from the within-dataset case using MPIIGaze dataset. Prior to the calibration, the uncertainty model would predict probability distribution far off from the true distribution, leading to the blue curve. The correctional regressor, R , samples a few points (black dots) from the testing data and learns the bias and overfitting behavior from the uncalibrated model, then coming up with the appropriate correction. After calibration with the help of the correction regressor R , the uncertainty model can predict uncertainties much more accurately (cyan dots) that follows the ideal curve (red dotted line). In the experiment with RTGene, the uncalibrated uncertainty model produces the blue curve relatively close to the ideal line with the uncalibrated uncertainty model, and in the experiment with

Table 2. Comparison of Angular Error, Average CPE for Evaluating Calibration

Training Dataset	Testing Dataset	Backbone	Average Angular Error (degree)		Average CPE (percent)		Error-Uncertainty Correlation
			Uncalibrated	Calibrated	Uncalibrated	Calibrated	Calibrated/ Uncalibrated
MPII	MPII	Resnet 18	5.88	4.71 (↓ 20%)	23.17	17.87 (↓ 23%)	0.20
RTGENE	RTGENE	Resnet 18	11.00	9.29 (↓ 16%)	19.62	17.83 (↓ 9%)	0.25
MPII	MPII	Resnet 50	6.04	4.65 (↓ 23%)	26.01	17.94 (↓ 31%)	0.09
RTGENE	RTGENE	Resnet 50	9.88	8.71 (↓ 12%)	22.70	17.51 (↓ 23%)	0.20
MPII	RTGENE	Resnet 18	13.42	11.33 (↓ 16%)	27.43	17.97 (↓ 34%)	0.05
RTGENE	MPII	Resnet 18	18.74	10.89 (↓ 42%)	19.72	16.27 (↓ 17%)	0.23
MPII	RTGENE	Resnet 50	13.82	11.28 (↓ 18%)	30.75	17.19 (↓ 44%)	0.04
RTGENE	MPII	Resnet 50	12.86	10.74 (↓ 16%)	24.67	19.47 (↓ 21%)	-0.10

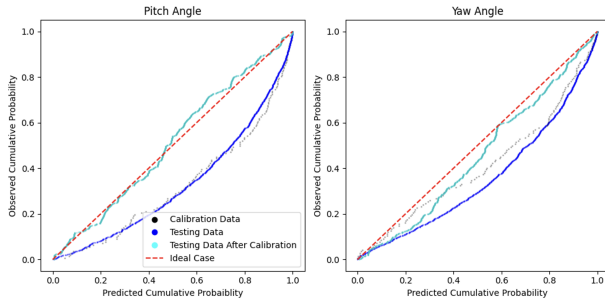


Figure 5. Visualization of correction effect of the calibration process. The calibration model learns the error behavior from a small subset (black dots) collected from testing data to learn model’s error behavior. During testing, the model can apply appropriate corrections to the uncalibrated uncertainty model such that the output from the correct model (cyan dots) matches the ideal case closer to reduce uncertainty error, rather than the high-error uncalibrated uncertainty inferences (blue dots).

MPII, the blue curve is relatively far away.

Angular prediction errors also experienced noticeable drops. We believe that this improvement was brought by the nonparametric nature of the correctional regressor. The original Gaussian distribution assumption may not necessarily agree with the true distribution, and thus, lead to relatively high errors relying on the mean value for angle inferences. The nonparametric correctional regressor allows the post-calibration model to take any distribution, allowing closer resemblance to the true distribution. Median values from the nonparametric, post calibration probability distribution, therefore, matches the true angular gaze values closer.

5.2. Variations in CPE and Angular Error

To further study the stability of uncertainty inferences, we plotted the distribution of CPE and angular error range from all testing cases with boxplots in Figure 6. Under all

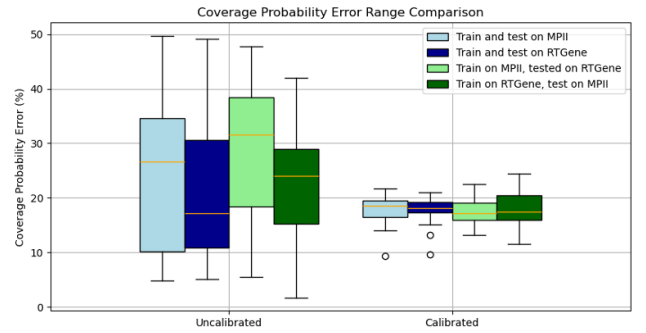


Figure 6. Boxplot showing the ranges of coverage probability error. Performances of uncalibrated models on uncertainty accuracy are much less consistent compared to the calibrated model. Orange line denotes the median value. Although some uncalibrated testing cases shows lower CPE, such event is not predictable.

circumstances, the calibrated uncertainty models produced much more consistent results compared to the uncalibrated ones. Although the lower bound for the CPE from the uncalibrated data is lower than that from the calibrated case, those ones are often unpredictable.

For angular prediction errors, no significant changes in ranges were observed other than reducing a couple of outliers in the testing with the uncalibrated models. We conclude that the most significant influence in angular uncertainties from the calibration is still the lowering of overall errors because of an more appropriate non-parametric probability model.

5.3. Case Study Results

For accurate uncertainty-aware models, we expect them to provide appropriate prediction ranges for the desired confidence interval. In this case study, we specified the confidence interval at 95% (2.5% to 97.5%) and we are expecting the prediction ranges to capture 95% of the label values across the entire testing cases. Table 3. summarizes the true

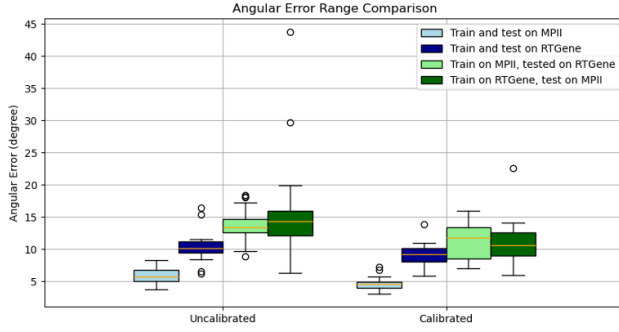


Figure 7. Boxplot showing the range of gaze angle prediction error. Changes in the error range are not uniform as reducing and stabilizing gaze angle prediction error is not the objective of uncertainty calibration although some extreme outliers were reduced. Calibration also demonstrated potential in increase angular prediction accuracies in uncertainty aware models.

inclusion rate in this case study.

By evaluating the true value include rate under the calibrated model column, we can see that the calibration process is successful in predicting close-to-desired prediction boundaries. It should be noted that to be counted for a successful inclusion, both pitch and yaw angles must fall within the prediction boundaries predicted by their perspective uncertainty models at the same time. Because the pitch and yaw uncertainty models are calibrated individually and independently, the final inclusion rate will be slightly lower than desired 95%, as shown in this case study.

The inclusion rate from the two baseline models shows that the uncertainty-aware models are significantly overconfident. While the models think they would capture 95% of the true values, but in reality, their capture rates are only half of their expectation. This much-below-expectation capture rate happens to both the uncalibrated heteroskedastic model that assumes Gaussian distribution and the non-parametric quantile regression. From this, we can conclude that errors in distribution assumption are not the primary contribution to the miscalibration problem.

Coupling the prediction ranges with the inclusion rate, we can conclude that both of these two baseline uncertainty-aware models are significantly overconfident. The prediction ranges are often much smaller than the calibrated models, yet the inclusion rates are significantly lower. Such over confidence issue could lead to severe trust loss if such system were to be applied in a high accuracy human-computer interaction system as the model will miss nearly half of the gaze tracking results.

It should be noted that there is one instance in the cross-dataset that with extremely large prediction range of 1.774, we believe this is caused by a sever overfitting and sharp difference between training and test data. Even with such large prediction range, its corresponding inclusion rate is

still significantly below the desired 0.95, demonstrating the unreliability of uncalibrated uncertainty models.

6. Conclusion

In this study, we first identify the need for a proper scoring metric for evaluating the uncertainty aware models in appearance-based gaze tracking. We pointed out that existing metric relies on a spurious correlation which cannot provide quantitatively evaluations. To meet this need, we proposed a strictly proper metric based on coverage probability that compared the predicted probability distribution to the observation. Being strictly proper, this metric will reaches the lowest value of 0 only when prediction exactly matches the observation.

We later identify the miscalibration problem from existing uncertainty model and introduced a remedy solution based on probability calibration. Testing results from a 3-fold cross-validation using two distinct datasets and two different backbone models demonstrate that the proposed remedy solution consistently mitigates the miscalibration problem, as evidenced by the newly introduced metric. Additionally, we also demonstrated the capability of correctly estimating the prediction boundaries with a case study that aims to estimate the prediction boundaries of a 95% confidence interval. Without calibration, the original models showed significant errors and overconfidence in the boundary estimation.

References

- [1] Charles Blundell, Julien Cornebise, Koray Kavukcuoglu, and Daan Wierstra. Weight uncertainty in neural network. In *Proceedings of the 32nd International Conference on Machine Learning*, pages 1613–1622, Lille, France, 2015. PMLR. 5
- [2] GLENN W. BRIER. Verification of forecasts expressed in terms of probability. *Monthly Weather Review*, 78(1):1–3, 1950. 2
- [3] Zhaokang Chen and Bertram E. Shi. *Appearance-Based Gaze Estimation Using Dilated-Convolutions*, pages 309–324. Springer International Publishing, 2019. 2
- [4] Zhaokang Chen, Didan Deng, Jimin Pi, and Bertram E. Shi. Unsupervised outlier detection in appearance-based gaze estimation. In *2019 IEEE/CVF International Conference on Computer Vision Workshop (ICCVW)*, pages 1088–1097. IEEE, 2019. 2
- [5] Tobias Fischer, Hyung Jin Chang, and Yiannis Demiris. *RT-GENE: Real-Time Eye Gaze Estimation in Natural Environments*, pages 339–357. Springer International Publishing, 2018. 2, 4
- [6] Yarin Gal and Zoubin Ghahramani. Dropout as a bayesian approximation: Representing model uncertainty in deep learning. In *international conference on machine learning*, pages 1050–1059. PMLR, 2016. 5

Table 3. Prediction Range and Inclusion Probability Comparison for the 95% Confidence Interval Case Study

Training Dataset	Testing Dataset	Backbone	Average Prediction Range (rad)			Gaze Angle Value Inclusion Probability (desired value:0.95)		
			Calibrated	Uncalibrated	Quantile Regression	Calibrated	Uncalibrated	Quantile Regression
MPII	MPII	Resnet 18	0.273	0.122	0.238	0.880	0.411	0.405
MPII	MPII	Resnet 50	0.305	0.213	0.262	0.883	0.590	0.381
RTGene	RTGene	Resnet 18	0.435	0.267	0.253	0.865	0.514	0.516
RTGene	RTGene	Resnet 50	0.487	0.242	0.265	0.888	0.506	0.503
MPII	RTGene	Resnet 18	0.584	0.174	0.301	0.867	0.478	0.343
MPII	RTGene	Resnet 50	0.649	0.253	0.315	0.890	0.485	0.340
RTGene	MPII	Resnet 18	0.641	0.683	1.774	0.887	0.637	0.523
RTGene	MPII	Resnet 50	0.600	0.419	0.224	0.886	0.462	0.164

- [7] Tilmann Gneiting and Adrian E Raftery. Strictly proper scoring rules, prediction, and estimation. *Journal of the American Statistical Association*, 102(477):359–378, 2007. [3](#)
- [8] Alex Graves. Practical variational inference for neural networks. In *Advances in Neural Information Processing Systems*. Curran Associates, Inc., 2011. [5](#)
- [9] Paris Her, Logan Manderle, Philippe A. Dias, Henry Medeiros, and Francesca Odone. Uncertainty-aware gaze tracking for assisted living environments. *IEEE Transactions on Image Processing*, 32:2335–2347, 2023. [2, 3](#)
- [10] Petr Kellnhofer, Adria Recasens, Simon Stent, Wojciech Matusik, and Antonio Torralba. Gaze360: Physically unconstrained gaze estimation in the wild. In *2019 IEEE/CVF International Conference on Computer Vision (ICCV)*, pages 6911–6920. IEEE, 2019. [2, 3](#)
- [11] Alex Kendall and Yarin Gal. What uncertainties do we need in bayesian deep learning for computer vision? *Advances in neural information processing systems*, 30, 2017. [2](#)
- [12] Volodymyr Kuleshov, Nathan Fenner, and Stefano Ermon. Accurate uncertainties for deep learning using calibrated regression. In *Proceedings of the 35th International Conference on Machine Learning*, pages 2796–2804. PMLR, 2018. [1, 2](#)
- [13] Balaji Lakshminarayanan, Alexander Pritzel, and Charles Blundell. Simple and scalable predictive uncertainty estimation using deep ensembles. *Advances in neural information processing systems*, 30, 2017. [1](#)
- [14] D.A. Nix and A.S. Weigend. Estimating the mean and variance of the target probability distribution. In *Proceedings of 1994 IEEE International Conference on Neural Networks (ICNN'94)*, pages 55–60 vol.1. IEEE, 1994. [5](#)
- [15] Seonwook Park, Shalini De Mello, Pavlo Molchanov, Umar Iqbal, Otmar Hilliges, and Jan Kautz. Few-shot adaptive gaze estimation. In *2019 IEEE/CVF International Conference on Computer Vision (ICCV)*, pages 9367–9376. IEEE, 2019. [2](#)
- [16] Francesca Pianosi and Thorsten Wagener. A simple and efficient method for global sensitivity analysis based on cumulative distribution functions. *Environmental Modelling & Software*, 67:1–11, 2015. [3](#)
- [17] Brian A. Smith, Qi Yin, Steven K. Feiner, and Shree K. Nayar. Gaze locking: passive eye contact detection for human-object interaction. In *Proceedings of the 26th Annual ACM Symposium on User Interface Software and Technology*, page 271–280, New York, NY, USA, 2013. Association for Computing Machinery. [2](#)
- [18] Yusuke Sugano, Yasuyuki Matsushita, and Yoichi Sato. Appearance-based gaze estimation using visual saliency. *IEEE Transactions on Pattern Analysis and Machine Intelligence*, 35(2):329–341, 2013. [2](#)
- [19] Xucong Zhang, Yusuke Sugano, Mario Fritz, and Andreas Bulling. Appearance-based gaze estimation in the wild. In *2015 IEEE Conference on Computer Vision and Pattern Recognition (CVPR)*, pages 4511–4520. IEEE, 2015. [1, 2, 4](#)
- [20] Xucong Zhang, Yusuke Sugano, Mario Fritz, and Andreas Bulling. It’s written all over your face: Full-face appearance-based gaze estimation. In *2017 IEEE Conference on Computer Vision and Pattern Recognition Workshops (CVPRW)*. IEEE, 2017. [2](#)
- [21] Wenqi Zhong, Chen Xia, Dingwen Zhang, and Junwei Han. Uncertainty modeling for gaze estimation. *IEEE Transactions on Image Processing*, 33:2851–2866, 2024. [1](#)